ELSEVIER

Mechanics of indentation of plastically graded materials—I: Analysis

I.S. Choi[1], M. Dao, S. Suresh*

Department of Materials Science and Engineering, Massachusetts Institute of Technology, Cambridge, MA 02139, USA

Abstract

The introduction of controlled gradients in plastic properties is known to influence the resistance to damage and cracking at contact surfaces in many tribological applications. In order to assess potentially beneficial effects of plastic property gradients in tribological applications, it is essential first to develop a comprehensive and quantitative understanding of the effects of yield strength and strain hardening exponent on contact deformation under the most fundamental contact condition: normal indentation. To date, however, systematic and quantitative studies of plasticity gradient effects on indentation response have not been completed. A comprehensive parametric study of the mechanics of normal indentation of plastically graded materials was therefore undertaken in this work by recourse to finite element method (FEM) computations. On the basis of a large number of computational simulations, a general methodology for assessing instrumented indentation response of plastically graded materials is formulated so that quantitative interpretations of depth-sensing indentation experiments could be performed. The specific case of linear variation in yield strength with depth below the indented surface is explored in detail. Universal dimensionless functions are extracted from FEM simulations so as to predict the indentation load versus depth of penetration curves for a wide variety of plastically graded engineering metals and alloys for interpretation of, and comparisons with, experimental results. Furthermore, the effect of plasticity gradient on the residual indentation pile-up profile is systematically studied. The computations reveal that pile-up of the graded alloy around the indenter, for indentation with increasing yield strength beneath the surface, is noticeably higher than that for the two homogeneous reference materials that constitute the bounding conditions for the graded material. Pile-up is also found to be an increasing function of yield strength gradient and a decreasing function of frictional coefficient. The stress and plastic strain distributions under the indenter tip with and without plasticity gradient are also examined to rationalize the predicted trends. In Part II of this paper, we compare the predictions of depth-sensing indentation and pile-up response with experiments on a specially made, graded model Ni–W alloy with controlled gradients in nanocrystalline grain size.
© 2007 Elsevier Ltd. All rights reserved.

Keywords: Indentation; Finite Element Method; Plastically graded materials; Pile-up; Hardness

---

*Corresponding author. Tel.: +1 617 253 3320; fax: +1 617 253 0868.
E-mail address: ssuresh@mit.edu (S. Suresh).
[1]Present address: Forschungszentrum Karlsruhe, Institute for Materials Research II, 76344 Karlsruhe, Germany.

1. Introduction

Over the past two decades, the study of graded materials and surfaces with controlled spatial variations in composition, microstructure and properties has evolved as an important topic in design for exceptional resistance to deformation, fracture, fatigue and tribological damage (e.g., Suresh and Mortensen, 1998; Suresh, 2001). The engineering of materials with graded microstructures dates back to the manufacture of ancient Japanese swords wherein the microstructure of the steel blades was optimized for a softer and tougher core and a hardened sharp edge (Smith, 1960). Major engineering applications involving the use of graded materials include carburizing, nitriding, ion implantation, and step-wise or continually graded thermal spray coatings (e.g., Suresh and Mortensen, 1998; Suresh, 2001).

Earlier studies (e.g., Hirai, 1996) of graded materials explored possibilities for enhanced performance in high-temperature applications in aerospace components, solid oxide fuel cells and energy conversion devices. However, the need to circumvent gradual changes in composition through diffusion over time inevitably calls for the use of graded materials in lower temperature applications. In this regard, a potentially important benefit of graded materials could be the suppression of cracking through optimal redistribution of stresses at surfaces and interfaces subjected to mechanical and tribological loading (Suresh and Mortensen, 1998). Frictionless normal indentation is a simple benchmark to characterize the mechanics of contact at surfaces through indenters of different tip geometries and to assess many fundamental characteristics of asperity contact as well as defect and crack nucleation at and beneath surfaces (Gerberich et al., 1996; Gouldstone et al., 2001; Suresh, 2006). Furthermore, depth-sensing instrumented indentation has become a widely adopted tool in recent years for the local probing of mechanical properties of thin-film, small-volume and bulk materials and surfaces over a variety of length scales (Freund and Suresh, 2003; Cheng et al., 2004; Gouldstone et al., 2007).

Analytical and computational results of the indentation load versus indenter penetration depth on a continuously graded surface with controlled gradients in elastic modulus have been developed for spherical, cylindrical and conical indenters (Giannakopoulos and Suresh, 1997). These studies reveal that when the elastic modulus increases in some controlled fashion as a function of depth below the indented surface, the tensile stresses that develop at the indenter contact perimeter can be redistributed to the elastically stronger material beneath the surface. A significant outcome of this stress redistribution is that the elastic material so graded becomes significantly more resistant to Hertzian cone crack formation during spherical indentation (Jitcharoen et al., 1998). Such beneficial effects also carry over to situations involving frictional sliding of a spherical indenter over the graded surface where the classical herringbone crack formation can be suppressed with appropriate modulus gradation (Suresh et al., 1999).[2]

The mechanics of indentation of materials with gradients in elastic modulus as a function of depth beneath the indented surface has been reasonably well studied (Giannakopoulos and Suresh, 1997; Jitcharoen et al., 1998; Suresh and Mortensen, 1998; Suresh et al., 1999; Suresh, 2001). However, indentation of plastically graded materials has remained a relatively unexplored topic because of the complexities associated with characterizing plastic deformation over a region in which the yield strength, strain hardening exponent, tensile strength, hardness and ductility could all vary spatially. This difficulty is further compounded by the fact that it is extremely challenging to produce model systems of plastically graded materials in sufficient quantities where the sole effects of gradients in a particular plastic property on overall indentation response could be systematically controlled and evaluated. The few preliminary reports of indentation of plastically graded materials (Nakamura et al., 2000; Suresh, 2001; Giannakopoulos, 2002; Gu et al., 2003; Cao and Lu, 2004) do not provide sufficiently complete information on the mechanics of indentation. It is, therefore, the objective of the present work to develop a comprehensive and quantitative mechanics framework for interpreting instrumented indentation of plastically graded ductile metals. The companion paper, Part II, describes the synthesis of a nanocrystalline Ni–W alloy with well-controlled gradients in plastic deformation characteristics

---

[2]Note that some specific spatial variations in mechanical properties result in an improvement in resistance to damage and failure during normal contact when compared to an appropriate reference homogeneous structure. However, it is also possible to exacerbate damage processes through different types of graded microstructures (Suresh and Mortensen, 1998; Suresh, 2001).

and also compares indentation experimental results on the graded alloy with predictions of the analysis given here (Choi et al., 2007).

2. Model setup

Contrary to the indentation of elastic materials, it is nearly impossible to derive explicit analytical expressions of the indentation response of elasto-plastic materials of engineering interest. Thus, many studies have utilized dimensional analysis to describe the indentation response of homogeneous elasto-plastic materials (see some recent studies and reviews on instrumented indentation in (Cheng and Cheng, 1998, 2004; Dao et al., 2001; Chollacoop et al., 2003; Oliver and Pharr, 2004; Cao et al., 2005; Ogasawara et al., 2005; Wang and Rokhlin, 2005; Cao and Huber, 2006; Gouldstone et al., 2007). The general framework to extract dimensionless functions can be applicable to any plastically graded materials with monotonic variation of plasticity.

In this study, the case of a linear gradient in yield strength (with no spatial variation in strain-hardening exponent) is investigated as the first step to establish fundamental framework and the first-order general trend. The underlying mechanics principles and computational procedure remain essentially the same for nonlinear gradients. Particular attention is devoted to the prediction of indentation force as a depth of penetration beneath the contact surface for the linearly graded material.

2.1. Problem formulation

Fig. 1(a) schematically shows the indentation of plastically graded materials with a conical indenter. A commonly used probe, the Berkovich indenter, is a three-sided pyramid indenter. The apex angle of the conical indenter was chosen to be $70.3°$ since it is known that this angle is analogous to the more common Berkovich indenter (e.g Oliver and Pharr, 1992; Gouldstone et al., 2007). Fig. 1(b) illustrates the profile of gradient in plasticity analyzed in this work.
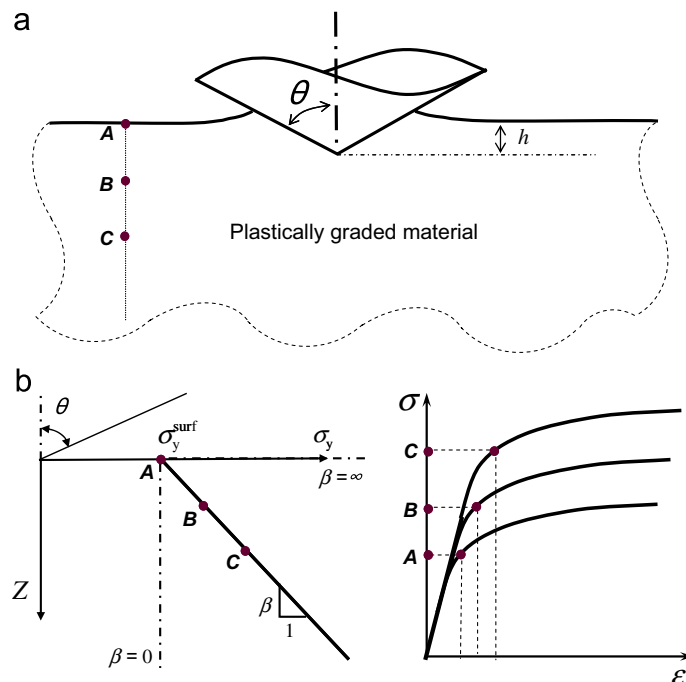

Fig. 1. (a) Schematic diagram of plastically graded materials under conical indentation. (b) Profile of linear gradient in yield strength in the direction of indentation depth Z and power laws of plastic deformation that governs each material point, A, B and C respectively.

The linear gradient in yield strength from the surface is defined as

$$\sigma_y(Z) = \sigma_y^{surf}(1 + \beta Z), \tag{1}$$

where β is named the index of gradient and Z is the depth from the surface. For $\beta = 0$, the homogeneous case is recovered, while for $\beta > 0$, the yield strength is increasing with depth and for $\beta < 0$, the yield strength is decreasing with depth. There are no spatial variations in material properties within planes parallel to the indented surface. The plastically graded material is also elastically homogeneous.

The elastic and plastic responses are approximated, respectively, by Hooke's law and the von Mises yield criterion with isotropic power law hardening. Under those general conditions, the dependence of the true stress σ on the true strain ε is commonly expressed as

$$\begin{cases} \sigma = E\varepsilon & (\sigma \leqslant \sigma_y), \\ \sigma = R\varepsilon^n & (\sigma \geqslant \sigma_y), \end{cases} \tag{2a,b}$$

where E is the Young's modulus, R the strength coefficient, σ_y the initial yield stress at zero offset strain and n the strain hardening exponent not varying with depth. In this representation, the true strain ε is a uniaxial strain. The multiaxial stress state for indentation simulations is introduced by replacing the uniaxial formulation of Eq. (2) with the appropriate von Mises effective stress and strain measures.

2.2. Computational model setup

An axisymmetric two-dimensional finite element model was constructed to simulate the indentation response of plastically graded materials. Fig. 2 shows the mesh design. The semi-infinite substrate of the indented solid was modeled using 8105 four-noded, bilinear axisymmetric quadrilateral elements. A fine mesh near the contact region and a gradually coarser mesh further from the contact region were used to ensure numerical accuracy. The dimension of the substrate is set large enough to ignore sensitivity of far field boundary conditions. The minimum number of contact elements in the contact zone was no less than 14 in each FEM computation. The indenter was modeled as a rigid body with the contact taken to be frictionless, unless otherwise noted. Large deformation FEM computations were performed using ABAQUS Standard (SIMULIA, Providence, RI, USA). A numerical subroutine was implemented that enables to assign individual material properties to the element level. Using the subroutine, the gradient of yield strength was introduced across the interface. For the purpose of testing the subroutine and verifying the mesh, the results of elastically graded materials were successfully reproduced both for conical indentation and for spherical indentation, and a mesh with 50% less elements in the contact region gives virtually the same load–displacement response.
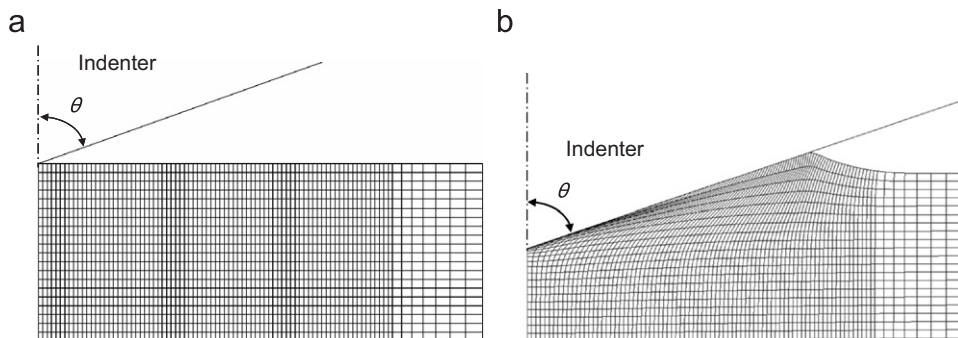

Fig. 2. Close-up view of the finite element mesh used for conical indentation simulations: (a) undeformed mesh and (b) deformed mesh.

3. Results

3.1. Load–displacement response with plasticity gradients

Fig. 3 shows typical computational load (P) versus indentation depth (h) curves for decreasing and increasing plasticity gradient cases and the reference homogeneous material. For all three cases, Young's modulus $E = 214$ GPa, the surface yield strength $\sigma_y^{\mathrm{surf}} = 587$ MPa and the strain hardening exponent $n = 0$. The index of gradient β is -0.006 and $0.06\,\mu\mathrm{m}^{-1}$, respectively, for the two decreasing and increasing gradient alloys. Using the nonlinear least-squares fitting, we fit a parabolic function $P = Ch^2$ to the homogeneous case ($R^2 = 0.99998$[3]). The homogeneous case, for which $\beta = 0$ is shown to obey the parabolic relationship where the loading curvature, $C = P/h^2$, is a constant independent of h. With the same surface properties as the homogeneous case, the decreasing gradient case bears less load and the increasing gradient case bears higher load at the same indentation depth, as compared to the homogeneous case. Both plastic gradient cases deviate from the ideal parabolic functional dependence for homogeneous materials. At a fixed indentation load P_0, the indenter penetration depth decreases as β increases from negative to positive values (Fig. 3).

3.2. Stress and strain distributions beneath the indenter

Fig. 4 shows the contours of constant von Mises effective stress around the indenter impression for decreasing plasticity gradient, homogeneous and increasing plasticity gradient case, respectively. The three cases are plotted at the same load of $P_0 = 3.33$ mN, and correspond to the indentation depths of h_1, h_2 and h_3, respectively, as shown in Fig. 3. Due to the high stress concentration near the indenter tip, the material below the indenter plastically yields and thus the von Mises stress distribution within the plastic zone corresponds to the linear yield stress gradient for both plastically graded cases. The highest von Mises stress occurs below the surface for the increasing gradient case, while for both the homogeneous case and decreasing gradient case the highest von Mises stress appears on the surface directly in contact with the indenter and immediately around the indentation impression.

Fig. 5 shows the maximum principal stress contours for decreasing plasticity gradient, homogeneous and increasing plasticity gradient case, at the same load of $P_0 = 3.33$ mN, and correspond to the indentation depths of h_1, h_2 and h_3, respectively, as shown in Fig. 3. Under the same indentation load, the volume of positive tensile tress is larger (smaller) for the decreasing (increasing) gradient case than the homogeneous case, while the largest tensile stress increases with increasing plasticity gradient β. For a sufficiently large positive value of β in Fig. 5(c), no tensile stress develops at the indented surface which is different from the homogeneous case as well as the decreasing gradient case. For the decreasing gradient case, the surface area experiencing positive tensile stresses increases with higher magnitude of the negative gradient.

Fig. 6 shows the equivalent plastic strain contours around the indenter impression for decreasing plasticity gradient, homogeneous and increasing plasticity gradient case, at the same load of $P_0 = 3.33$ mN, and correspond to the indentation depths of h_1, h_2 and h_3, respectively, as shown in Fig. 3. Under the same indentation load, the plastic zone size is larger (smaller) for the decreasing (increasing) gradient case than the homogeneous case, respectively. However, if one compares the maximum values of plastic strain (not shown in the figure), higher plastic strains occur near the indenter tip in the increasing gradient case than the homogenous case, while lower plastic strains accumulate under the indenter in the decreasing gradient case than the homogeneous case. Thus, higher plastic strains accumulate under the indenter over a smaller plastic zone with increasing (positive) plasticity gradient, resulting higher pile-up ratio than the homogeneous case, which will be shown later in Section 3.4.

We have also compared plastic strain distribution of the three cases shown in Fig. 3, all at the same 7 µm indentation depth (figure not shown). The observed trend is exactly the same as that shown in Fig. 6, although the relative differences between the plastic zone sizes are apparently smaller in this case when the strain distribution maps are plotted at the same indentation depth.

---

[3]The R^2 is a measure of how well the regression line represents the data, defined as $R^2 = 1 - (\sum(Y_D - Y_F)^2)/(\sum(Y_D - \bar{Y}_D)^2)$, where Y_D is data and Y_F is the fitting function.
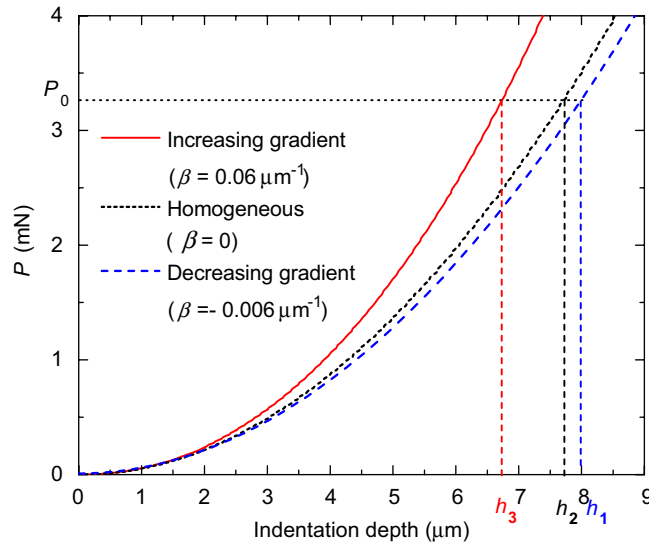
Fig. 3. Typical load (P) versus indentation depth (h) responses for decreasing plasticity gradient, homogeneous and increasing plasticity gradient cases, respectively. For all three cases, Young's modulus $E = 214$ GPa, the surface yield strength $\sigma_y^{surf} = 587$ MPa and the strain hardening exponent $n = 0$.
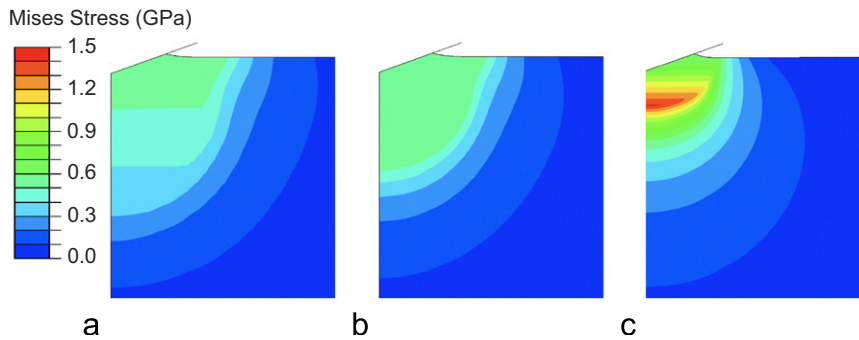

Fig. 4. Typical Mises stress distribution maps for (a) decreasing plasticity gradient, (b) homogeneous case and (c) increasing plasticity gradient case, respectively. The three cases are plotted at the same load of $P_0 = 3.33$ mN, and correspond to the indentation depths of h_1, h_2 and h_3, shown in Fig. 3.
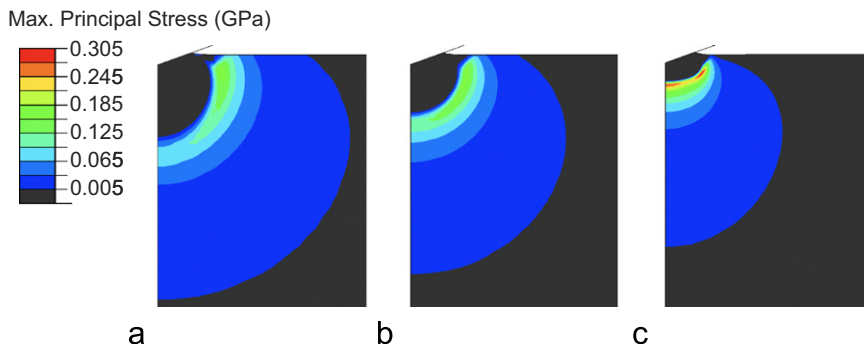

Fig. 5. Typical maximum principal stress distribution maps for (a) decreasing plasticity gradient, (b) homogeneous case and (c) increasing plasticity gradient case, respectively. The three cases are plotted at the same load of $P_0 = 3.33$ mN, and correspond to the indentation depths of h_1, h_2 and h_3, respectively, as shown in Fig. 3.
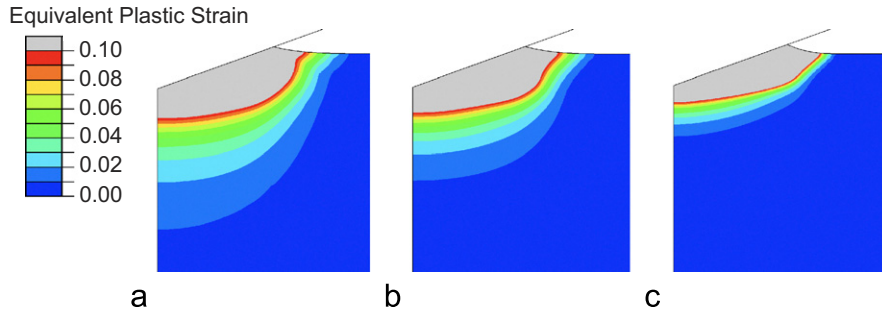
Fig. 6. Typical equivalent plastic strain distribution maps for (a) decreasing plasticity gradient, (b) homogeneous case and (c) increasing plasticity gradient case, respectively. The three cases are plotted at the same load of $P_0 = 3.33\,\text{mN}$, and correspond to the indentation depths of h_1, h_2 and h_3, shown in Fig. 3.

3.3. Dimensional analysis and universal dimensionless functions

Now, we will extract a dimensionless function to predict indentation curve for plastically graded materials with increasing linear gradient in yield strength. As mentioned in Section 2, the general framework of the dimensional analysis can be applicable to any plastically graded materials with monotonic variation of plasticity.

For a self-similar sharp indenter (conical, Berkovich or Vickers, with fixed indenter shape and tip angle) indenting normally into a plasticity gradient, the load P depends on material properties and geometrical variables:

$$P = P(h, E^*, \sigma_y^{\text{surf}}, n, \beta, \theta), \tag{3}$$

where h denotes the indentation depth; E^* is the reduced elastic modulus; σ_y^{surf} is the yield strength at surface; n is the strain hardening exponent; β is the measure of the yield strength gradation as defined in Eq. (1); and θ is the half apex angle of the conical indenter. For a fixed tip angle, five-dimensional variables are required to describe indentation load. However, it is practically impossible to perform parametric studies to cover all the engineering materials. For example, six different values of elastic constants, surface yield strengths, hardening exponents and index of gradient require 1296 simulations to be performed. Therefore, dimensional analysis is used with the smallest number of independent variables so that dimensionless functions can be obtained for a wide range of parametric space with the least effort. In addition, the dimensionless relation provides fundamental understanding of self-similarity and scaling with respect to each dimensionless variable.

Applying the Pi theorem in dimensional analysis (Taylor, 1974) for a fixed indenter apex angle, the load P can be represented by the dimensionless function:

$$\frac{P}{E^* h^2} = \Pi(\varepsilon_y^*, n, \beta h), \tag{4}$$

where $\varepsilon_y^* = \sigma_y^{\text{surf}}/E^*$. The number of arguments is now reduced to three independent governing dimensionless parameters instead of five-dimensional variables. Define the indentation curvature C as

$$C = \frac{P}{h^2}. \tag{5}$$

For plastically graded case, $C = C_g$ is a function of indentation depth h. It should be noted that the parabolic variation of indentation load with depth of penetration typically seen in homogeneous elasto-plastic materials subjected to sharp indentation breaks down for graded materials. Furthermore, the mean contact pressure is a function of indentation depth as well since β introduces a new length scale to the indentation problem.

Fig. 7 shows a set of representative simulation results plotting $(C_g - C_H)/(C_{\text{dfc}}^* - C_H)$ covering a wide range of βh, where C_g is the curvature of plastically graded materials for indentation by a rigid conical indenter; C_{dfc}^* is the indentation curvature of an elastic-half space by a rigid conical indenter; C_H is the indentation curvature
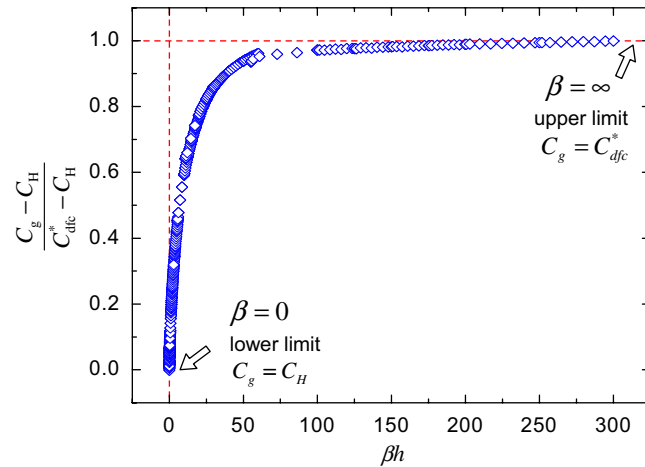
Fig. 7. Plot of $(C_{\mathrm{g}} - C_{\mathrm{H}})/(C^*_{\mathrm{dfc}} - C_{\mathrm{H}})$ for plastically graded materials with $E = 214\,\mathrm{GPa}$, $n = 0.1$, $\sigma_{\mathrm{y}}^{\mathrm{surf}} = 783\,\mathrm{MPa}$ in the wide range of βh. Two analytical limits are shown.
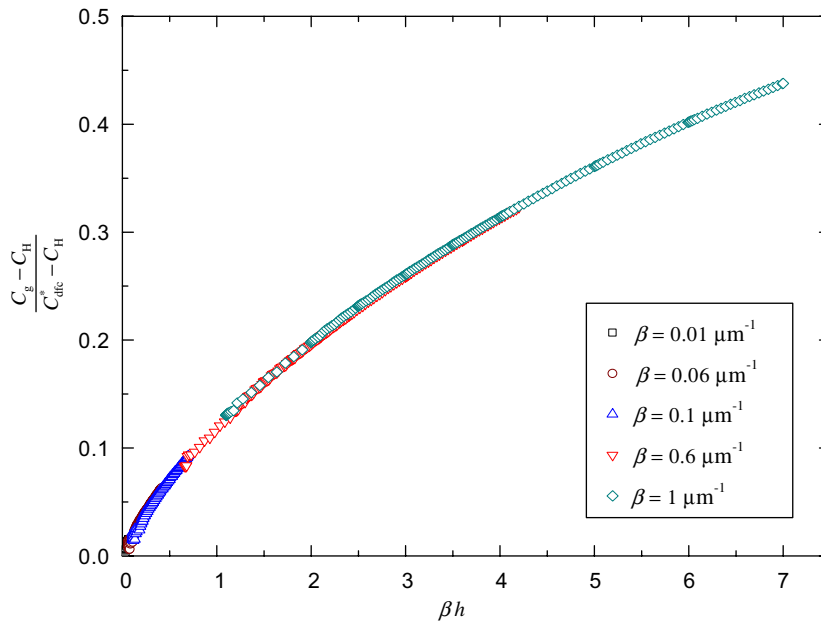
Fig. 8. Plot of $(C_{\mathrm{g}} - C_{\mathrm{H}})/(C^*_{\mathrm{dfc}} - C_{\mathrm{H}})$ versus βh for plastically graded materials with $E = 214\,\mathrm{GPa}$, $n = 0$, $\sigma_{\mathrm{y}}^{\mathrm{surf}} = 783\,\mathrm{MPa}$ and six different β values. The overlap of all studied cases is clearly observed.

of elasto-plastic homogeneous materials by a rigid conical indenter at the surface as point A in Fig. 1. As $\beta h \to 0$, $(C_{\mathrm{g}} - C_{\mathrm{H}})/(C^*_{\mathrm{dfc}} - C_{\mathrm{H}}) \to 0$, as anticipated, and this limiting case corresponds to the indentation curvature of a homogeneous material. When $\beta h \to \infty$, $(C_{\mathrm{g}} - C_{\mathrm{H}})/(C^*_{\mathrm{dfc}} - C_{\mathrm{H}}) \to 1$, and this limiting case corresponds to the indentation curvature of an elastic half space.

We now examine functional dependence of the three independent dimensionless variables, $\varepsilon_{\mathrm{y}}^*$, n and βh in the context of indentation. In order to ensure that βh provides a unique description of indentation curvature for arbitrary variations in β and h, it is necessary to establish that all computed values of the function $(C_{\mathrm{g}} - C_{\mathrm{H}})/(C^*_{\mathrm{dfc}} - C_{\mathrm{H}})$ with different plasticity gradients β should collapse into a single curve for all variations in h. This is demonstrated in the results plotted in Fig. 8. Although the overlap of different β values are shown here with βh ranging from zero to seven, the scaling behavior should be valid for the entire range of

βh up to at least 300 as shown in Fig. 7. The same scaling behavior shown in Figs. 7 and 8 are also validated using different hardening exponents spanning from 0 to 0.5.

Since the explicit close-form dimensionless functions for homogeneous elastic case (Johnson, 1985; Fischer-Cripps, 2000) and elasto-plastic cases (Dao et al., 2001) are available in the literature, C_{dfc}^* and C_H can be considered known or readily available using established methods. If the dimensionless function,

$$\Pi_C = \frac{C_g - C_H}{C_{\text{dfc}}^* - C_H}, \tag{6}$$

is known, then the indentation curvature C_g can be obtained using Eq. (6). Consequently, the entire load (P) versus indentation depth (h) curve can be obtained using Eq. (5).

Note that $0 \leqslant (C_g - C_H)/(C_{\text{dfc}}^* - C_H) \leqslant 1$ (see Fig. 7). Without any loss of generality, Π_C can be expressed as

$$\Pi_C = \frac{C_g - C_H}{C_{\text{dfc}}^* - C_H} = 1 - g_{\text{re}}, \tag{7}$$

where $0 \leqslant g_{\text{re}} \leqslant 1$. By rearranging Eq. (7), the size dependence of indentation curvature of plastically graded materials is expressed by a rule-of-mixture type formulation:

$$C_g = C_{\text{dfc}}^*(1 - g_{\text{re}}) + C_H g_{\text{re}}. \tag{8}$$

Thus, the problem is reduced to the determination of the following dimensionless function:

$$g_{\text{re}} = \Pi_{\text{re}}(\varepsilon_y^*, n, \beta h). \tag{9}$$

A comprehensive parametric study of 320 elasto-plastic cases was conducted (see Appendix for details). This study covered nanocrystalline (nc) materials in addition to common engineering metals with the values of $\varepsilon_y^* = \sigma_y^{\text{surf}}/E^*$ varied over the range of 2.13×10^{-4} to 4.67×10^{-2}. The strain hardening exponent, n, varied from 0 to 0.5, and Poisson ratio was fixed as $\nu = 0.3$. Five different increasing gradients for β between 0.01 and 1 were computed.

In order to map these 320 cases with respect to the three independent dimensionless variables, ε_y^*, n and βh, the stretched exponential functional form is chosen to represent g_{re} in Eq. (9):

$$g_{\text{re}} = \exp[-(k\beta h)^d], \tag{10}$$

where $k = k(\varepsilon_y^*, n)$ and $d = d(\varepsilon_y^*, n)$ are dimensionless parameters. Eq. (10) is selected since it satisfies the asymptotic conditions, $0 \leqslant g_{\text{re}} \leqslant 1$, and fits all the simulation results very well. In addition, the stretched exponential function is widely used to describe many of quasi-static thermodynamic phenomena or statistical distributions (Williams, 1970; Chamberlin et al., 1984; Kakalios et al., 1987; Malacarne et al., 2001, 2002; Picoli et al., 2003). Combining Eqs. (4), (5), (8) and (10), the dimensionless functional form of normalized load is written by

$$\Pi = \frac{P}{E^* h^2} = \frac{C_g}{E^*} = \frac{C_{\text{dfc}}^*}{E^*} \left[(1 - \exp(-(k(\beta h))^d) \right] + \frac{C_H}{E^*} \exp(-(k(\beta h))^d). \tag{11}$$

Here C_{dfc}^* is the indentation curvature of an elastic-half space by a rigid conical indenter:

$$C_{\text{dfc}}^* = \delta \frac{2E^* \tan \theta}{\pi}, \tag{12}$$

where $\delta = 1.0553$ was obtained via simulations for the apex angle of $\theta = 70.3°$. In Eq. (11), C_H is the indentation curvature of elasto-plastic homogeneous materials by a rigid conical indenter at the surface, indicated as point A in Fig. 1. The dimensionless function for the homogeneous case is known from the literature (Dao et al., 2001; Cao et al., 2005; Ogasawara et al., 2005; Wang and Rokhlin, 2005). For example, under frictionless condition, the previously developed functions in Dao et al. (2001) for homogeneous elasto-plastic cases can be used to obtain C_H in Eq. (11) as long as the available functions are accurate in the range of interest. Nevertheless, in this study, we used a different fitting function for C_H, Eq. (A.3), to encompass a much wider range of material parameters as described in the Appendix.

In order to determine the Π-function in Eq. (11), it is necessary to extract the function $g_{\text{re}} = \exp[-(k\beta h)^d]$ in Eq. (10), with respect to the governing dimensionless parameters ε_y^*, n and βh. In this regard, the closed form

dimensionless function was identified as follows. First, g_{re} was plotted with respect to the dimensionless parameter, βh, for each set of parameters n and ε_y^*. Using a sequence of nonlinear-regression fitting procedures, the values of k and d were determined for each case and then plotted in terms of ε_y^* for every different value of the parameter, n. By additional fitting procedures, the functional dependence of k and d with respect to n were determined using the selected fitting functions. Putting these dimensionless functional forms together led to a complete closed form dimensionless function of indentation response of plastically graded materials. A complete set of coefficients for the universal dimensionless function for indentation response of plastically graded materials with linear increasing gradient is listed in the Appendix. To validate the constructed universal function, we have compared the predictions from the universal function with a number of additional FEM simulation results which were not used as the fitting data points for the closed form dimensionless function. For example, for the four cases with $E = 214\,\text{GPa}$, $\sigma_y = 783\,\text{MPa}$, $\beta = 0.06\,\mu\text{m}^{-1}$, $n = 0.05, 0.25, 0.35$ and 0.45, the maximum difference in load versus displacement responses was found to be less than 3.5%.

It is noted that, with this closed form dimensionless function, the plastic gradient can be evaluated if the elasto-plastic properties of the surface material are known. The surface material property can be extracted by first performing a sufficiently shallow indentation and applying the reverse algorithms available in the literature (Gouldstone et al., 2007).

3.4. Pile-up behavior

Because of pile-up and sink-in, the true contact area can be either underestimated or overestimated by as much as 60% for indentation with a rigid conical indenter (Bolshakov and Pharr, 1998). Thus, the pile-up and sink-in behavior of indentation of homogeneous materials has been investigated by many researchers to quantify the pile-up and sink-in factors to extract accurate hardness values from the indentation (Cheng and Cheng, 2004; Wang and Rokhlin, 2005). The pile-up behavior for plastically graded materials, however, has hitherto not been studied.

Fig. 9 shows the schematic drawing of an indentation pile-up profile after complete unloading, where h_p is the pile-up height, h_r is the residual indentation depth and a_r is the residual indentation impression radius. For the sharp indentation of homogeneous materials, the ratio of the pile-up height (h_p) to the residual indentation depth (h_r) is not a function of the indentation depth due to geometrical self-similarity. For plastically graded materials, on the other hand, the ratio is not a constant, but it varies as a function of the indentation depth, h, and the plasticity gradient, β.

Fig. 10 shows the calculated pile-up ratio, h_p/h_r, for the plastically graded material, homogeneous surface material with $\sigma_y = \sigma_y^{\text{surf}}$, and homogeneous material below surface with $\sigma_y = 2.75\sigma_y^{\text{surf}}$, for an increasing yield strength gradient $\beta = 0.05\,\mu\text{m}^{-1}$. For all cases shown in this figure, the maximum indentation height before unloading is 3.5 μm. Figs. 10(a) and (b) show the results under frictionless condition and with frictional coefficient $\mu = 0.15$, respectively. As expected, the pile-up ratio is a decreasing function of σ_y/E^* for both plastically graded and homogeneous cases. However, the pile-up ratio of the graded material is shown to be noticeably higher than those for the two homogeneous reference materials that constitute the bounding conditions for the graded material. This rather non-intuitive result is expected to be related to the higher
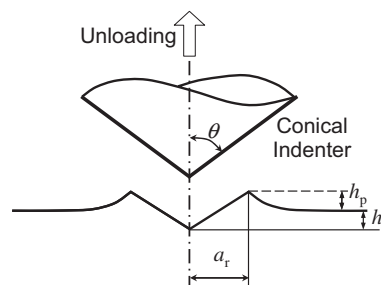

Fig. 9. Schematic drawing of an indentation pile-up profile after complete unloading.
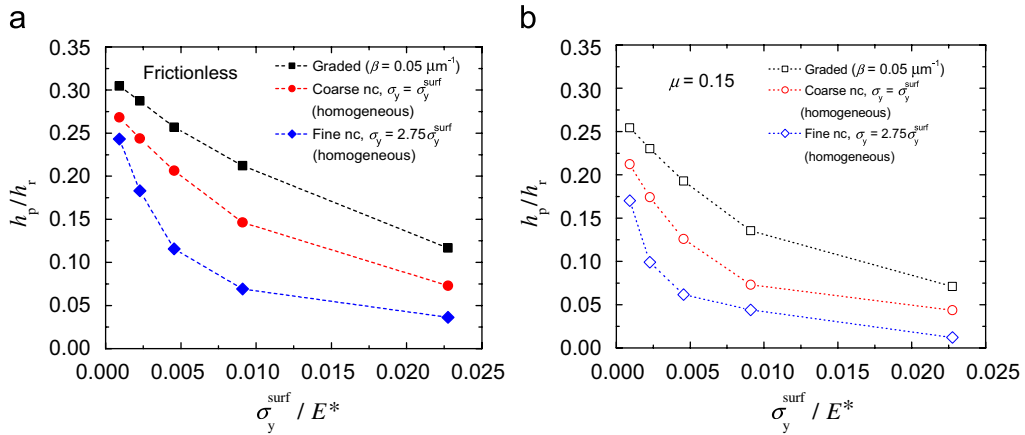
Fig. 10. Computed pile-up ratios for plastically graded material, homogeneous surface material with $\sigma_y = \sigma_y^{surf}$ and homogeneous material below surface with $\sigma_y = 2.75\sigma_y^{surf}$, respectively, for an increasing gradient $\beta = 0.05\,\mu m^{-1}$. For all cases shown in the figure, the maximum indentation height before unloading is $3.5\,\mu m$: (a) frictionless and (b) with frictional coefficient $\mu = 0.15$.
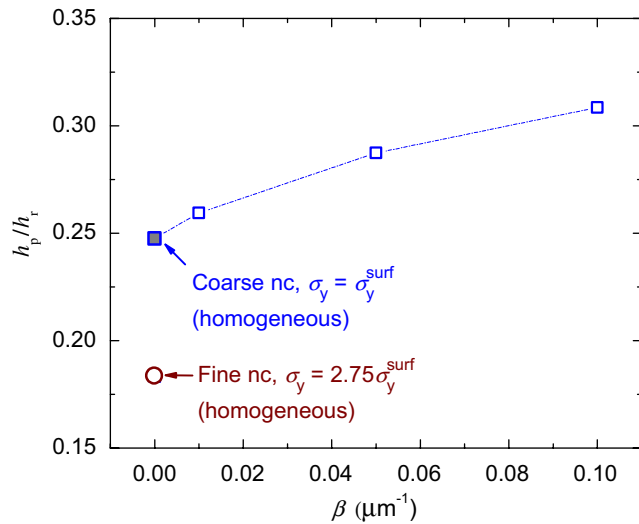

Fig. 11. Computed pile-up ratio versus plasticity gradient β ($\beta > 0$) for $\sigma_y/E^* = 0.00228$. Two homogeneous cases, with $\sigma_y = \sigma_y^{surf}$ and $2.75\sigma_y^{surf}$, are also shown for comparison. For all cases shown in the figure, the maximum indentation height before unloading is $3.5\,\mu m$.

plastic strain accumulated within the plastic zone near the indentation impression shown in Fig. 6. The increasing plasticity gradient redistributes the plastic strain closer to the surface around the indentation impression. Compare Fig. 10(a) with Fig. 10(b), frictional force is found to noticeably reduce the pile-up height.

Fig. 11 shows the computed pile-up ratio versus plasticity gradient β ($\beta > 0$) for $\sigma_y/E^* = 0.00228$. Two homogeneous cases, with $\sigma_y = \sigma_y^{surf}$ and $2.75\sigma_y^{surf}$, are also shown for comparison. Again, the maximum indentation height before unloading for all cases is $3.5\,\mu m$. Within the studied range of plasticity gradients, the pile-up ratio clearly increases with increasing gradient β. Again, pile-up ratios of the graded materials are always higher than that for the two homogeneous reference materials that constitute the bounding conditions for the graded material. With a number of preliminary simulations, we found that the pile-up ratio decreases with decreasing gradient β which is different from the increasing gradient case. More comprehensive studies on the decreasing gradient case are needed to obtain a more quantitative understating.

4. Concluding remarks

This paper describes the results of a comprehensive study of the mechanics of indentation of plastically graded metals with a linear gradient in yield strength, and no variation in elastic modulus and strain hardening exponent, beneath the indented surface. Key conclusions of this work are summarized as follows:

1. A universal dimensionless function describing the indentation response for the specific case of a linear gradient in yield strength is formulated. The form of the universal dimensionless function is obtained by performing a systematic parametric study using finite element analysis. This universal dimensionless function can be applied to elasto-plastic materials in general, whereas previous studies were limited to specific material classes and parameter sets.
2. Stress and strain fields produced by the indentation of the plastically graded material were studied. For a sufficiently large positive yield strength gradient β, no tensile stress develops at the indented surface which is different from the homogeneous case as well as the decreasing gradient case. With the same maximum load, the plastic zone volume decreases with increasing yield strength gradient β.
3. The effect of plasticity gradient on the residual indentation pile-up profile is systematically examined. The pile-up of the graded material around the indenter, for indentation with increasing yield strength beneath the surface, is found to be higher than that for the two homogeneous reference materials that constitute the bounding conditions for the graded material. Pile-up is also found to be an increasing function of yield strength gradient β and a decreasing function of frictional coefficient.

In Part 2 of this paper (Choi et al., 2007), the universal dimensionless function for linearly graded plastic properties is verified by indentation experiments on a graded nc Ni–W alloy. The experimentally measured pile-up is also shown to be consistent with the trend identified computationally.

Acknowledgements

Appendix

The functional form, Eq. (11), used to construct the closed-form universal dimensionless function for indentation response of plastically graded materials with linear increasing gradient is

$$\Pi = \frac{P}{E^* h^2} = \frac{C_g}{E^*} = \frac{C_{dfc}^*}{E^*}\left[(1 - \exp(-(k(\beta h))^d)\right] + \frac{C_H}{E^*}\exp(-(k(\beta h))^d). \tag{A.1}$$

Here C_{dfc}^* is the indentation curvature of an elastic-half space by a rigid conical indenter:

$$C_{dfc}^* = \delta\frac{2E^* \tan\theta}{\pi}, \tag{A.2}$$

where $\delta = 1.0553$ was obtained via simulations for the apex angle of $\theta = 70.3°$. The indentation curvature, C_H, for the elasto-plastic homogeneous material at the surface was obtained in this study using a different fitting function other than the ones used in the literature (e.g., Dao et al., 2001) to encompass a much wider range of material parameter space:

$$\frac{C_H}{E^*} = A_0 + (A_1 - A_0)\exp(-(A_2\varepsilon_y^*)^{A_3}), \tag{A.3a}$$

$$A_i = \sum_{j=0}^{5} A_{ij} n^j \quad (i = 0, 1, 2, 3), \tag{A.3b}$$

where n is the strain hardening exponent, and the coefficients of A_i are listed in Table A1.

The coefficients of k and d in Eq. (A.1) are dimensionless functions expressed within the following range:

$$2.13 \times 10^{-4} \leqslant \varepsilon_y^* \leqslant 4.67 \times 10^{-2} \tag{A.4}$$

and

$$0 \leqslant n \leqslant 0.5. \tag{A.5}$$

The following fitting function for k was used:

$$k = k_0 + k_1 \ln \varepsilon_y^* + k_2 \ln^2 \varepsilon_y^* + k_3 \ln^3 \varepsilon_y^*, \tag{A.6a}$$

$$k_i = \sum_{j=0}^{3} K_{ij} n^j, \tag{A.6b}$$

where n is the strain hardening exponent, and the coefficients of k_i are listed in Table A2.

The fitting function used for d was

$$d = d_0 + d_1 \ln \varepsilon_y^* + d_2 \ln^2 \varepsilon_y^* + d_3 \ln^3 \varepsilon_y^*, \tag{A.7a}$$

$$d_i = \sum_{j=0}^{3} D_{ij} n^j, \tag{A.7b}$$

where n is the strain hardening exponent, and the coefficients of d_i are listed in Table A3.

Table A1
Coefficients of Eq. (A.3)

Coefficients of A_0		Coefficients of A_1		Coefficients of A_2		Coefficients of A_3	
A_{00}	1.3354	A_{10}	−0.002530	A_{20}	70.7313	A_{30}	0.9536
A_{01}	7.1992	A_{11}	−0.3226	A_{21}	−458.2405	A_{31}	−2.6619
A_{02}	−60.2183	A_{12}	4.7091	A_{22}	4170.9546	A_{32}	18.9695
A_{03}	264.4932	A_{13}	−26.1686	A_{23}	−17579.8138	A_{33}	−87.6404
A_{04}	−530.0236	A_{14}	58.9110	A_{24}	34056.2417	A_{34}	181.0500
A_{05}	390.9552	A_{15}	−45.4883	A_{25}	−24424.7583	A_{35}	−135.6583

Table A2
Coefficients of Eq. (A.6)

		Coefficients of k_0		Coefficients of k_1		Coefficients of k_2		Coefficients of k_3	
$0 \leqslant n \leqslant 0.3$	K_{00}	9.1807	K_{10}	4.2482	K_{20}	0.6634	K_{30}	0.03481
	K_{01}	−74.9029	K_{11}	−40.2169	K_{21}	−7.0941	K_{31}	−0.4121
	K_{02}	602.2585	K_{12}	314.5440	K_{22}	54.4175	K_{32}	3.1180
	K_{03}	−1371.9050	K_{13}	−709.5667	K_{23}	−121.6850	K_{33}	−6.9183
$0.3 \leqslant n \leqslant 0.5$	K_{00}	37.5620	K_{10}	18.8629	K_{20}	3.1518	K_{30}	0.1750
	K_{01}	−260.9178	K_{11}	−136.0282	K_{21}	−23.3900	K_{31}	−1.3280
	K_{02}	654.4835	K_{12}	341.6410	K_{22}	58.8830	K_{32}	3.3525
	K_{03}	−530.3133	K_{13}	−276.6850	K_{23}	−47.6683	K_{33}	−2.7150

Table A3
Coefficients of Eq. (A.7)

	Coefficients of d_0		Coefficients of d_1		Coefficients of d_2		Coefficients of d_3	
$0 \leqslant n \leqslant 0.3$	D_{00}	1.1007	D_{10}	0.1891	D_{20}	0.02898	D_{30}	0.001010
	D_{01}	8.0143	D_{11}	3.7748	D_{21}	0.5558	D_{31}	0.02872
	D_{02}	86.9535	D_{12}	45.0585	D_{22}	7.8760	D_{32}	0.4550
	D_{03}	−374.8517	D_{13}	−191.4767	D_{23}	−32.5267	D_{33}	−1.8317
$0.3 \leqslant n \leqslant 0.5$	D_{00}	22.2812	D_{10}	10.8980	D_{20}	1.8146	D_{30}	0.0995
	D_{01}	−168.8878	D_{11}	−85.5364	D_{21}	−14.3082	D_{31}	−0.7896
	D_{02}	443.2770	D_{12}	224.1275	D_{22}	37.5025	D_{32}	2.0765
	D_{03}	−381.4817	D_{13}	−192.6517	D_{23}	−32.2600	D_{33}	−1.7917

References

Bolshakov, A., Pharr, G.M., 1998. Influences of pileup on the measurement of mechanical properties by load and depth sensing indentation techniques. J. Mater. Res. 13 (4), 1049–1058.

Cao, Y.P., Huber, N., 2006. Further investigation on the definition of the representative strain in conical indentation. J. Mater. Res. 21 (7), 1810–1821.

Cao, Y.P., Lu, J., 2004. A new scheme for computational modeling of conical indentation in plastically graded materials. J. Mater. Res. 19 (6), 1703–1716.

Cao, Y.P., Qian, X.Q., Lu, J., Yao, Z.H., 2005. An energy-based method to extract plastic properties of metal materials from conical indentation tests. J. Mater. Res. 20 (5), 1194–1206.

Chamberlin, R.V., Mozurkewich, G., Orbach, R., 1984. Time decay of the remanent magnetization in spin-glasses. Phys. Rev. Lett. 52 (10), 867–870.

Cheng, Y.-T., Cheng, C.-M., 1998. Scaling approach to conical indentation in elastic–plastic solids with work hardening. J. Appl. Phys. 84 (3), 1284.

Cheng, Y.T., Cheng, C.M., 2004. Scaling, dimensional analysis, and indentation measurements. Mater. Sci. Eng. R 44 (4–5), 91–149.

Cheng, Y.-T., Page, T., Pharr, G.M., Swain, M.V., Wahl, K.J.E., 2004. Special focus issue: fundamentals and applications of instrumented indentation in multidisciplinary research. J. Mater. Res. 19 (1).

Choi, I.S., Detor, A.J., Schwaiger, R., Dao, M., Schuh, C.A., Suresh, S., 2007. Indentation of plastically graded materials: II. Experiments on nanocrystalline alloys with grain-size Gradients. J. Mech. Phys. Solids, in press, doi:10.1016/j.jmps.2007.07.006.

Chollacoop, N., Dao, M., Suresh, S., 2003. Depth-sensing instrumented indentation with dual sharp indenters. Acta Mater. 51 (13), 3713–3729.

Dao, M., Chollacoop, N., Van Vliet, K.J., Venkatesh, T.A., Suresh, S., 2001. Computational modeling of the forward and reverse problems in instrumented sharp indentation. Acta Mater. 49 (19), 3899–3918.

Fischer-Cripps, A.C., 2000. Introduction to Contact Mechanics. Springer-Verlag, New York.

Freund, L.B., Suresh, S., 2003. Thin Film Materials: Stress, Defect Formation and Surface Evolution. Cambridge University Press, Cambridge, UK.

Gerberich, W.W., Nelson, J.C., Lilleodden, E.T., Anderson, P., Wyrobek, J.T., 1996. Indentation induced dislocation nucleation: the initial yield point. Acta Mater. 44 (9), 3585–3598.

Giannakopoulos, A.E., 2002. Indentation of plastically graded substrates by sharp indentors. Int. J. Solids Struct. 39 (9), 2495–2515.

Giannakopoulos, A.E., Suresh, S., 1997. Indentation of solids with gradients in elastic properties .2. Axisymmetric indenters. Int. J. Solids Struct. 34 (24), 2393.

Gouldstone, A., Van Vliet, K.J., Suresh, S., 2001. Nanoindentation-simulation of defect nucleation in a crystal. Nature 411 (6838), 656.

Gouldstone, A., Chollacoop, N., Dao, M., Li, J., Minor, A.M., Shen, Y.-L., 2007. Overview: indentation across size scales and disciplines: recent developments in experimentation and modeling. Acta Mater. 55 (12), 4015–4039.

Gu, Y., Nakamura, T., Prchlik, L., Sampath, S., Wallace, J., 2003. Micro-indentation and inverse analysis to characterize elastic-plastic graded materials. Mater. Sci. Eng. A 345 (1–2), 223–233.

Hirai, T., 1996. In: R.J. Brook (Ed.), Materials Science and Technology: A Comprehensive Treatment, Vol. 17B, Part 2. VCH, Weinheim, Germany, pp. 293–341.

Jitcharoen, J., Padture, N.P., Giannakopoulos, A.E., Suresh, S., 1998. Hertzian-crack suppression in ceramics with elastic-modulus-graded surfaces. J. Am. Ceram. Soc. 81 (9), 2301–2308.

Johnson, K.L., 1985. Contact Mechanics. Cambridge University Press, London.

Kakalios, J., Street, R.A., Jackson, W.B., 1987. Stretched-exponential relaxation arising from dispersive diffusion of hydrogen in amorphous-silicon. Phys. Rev. Lett. 59 (9), 1037–1040.

Malacarne, L.C., Mendes, R.S., Pedron, I.T., Lenzi, E.K., 2001. Nonlinear equation for anomalous diffusion: unified power-law and stretched exponential exact solution. Phys. Rev. E 6303 (3).

Malacarne, L.C., Mendes, R.S., Lenzi, E.K., 2002. q-exponential distribution in urban agglomeration. Phys. Rev. E 65 (1).

Nakamura, T., Wang, T., Sampath, S., 2000. Determination of properties of graded materials by inverse analysis and instrumented indentation. Acta Mater. 48 (17), 4293–4306.

Ogasawara, N., Chiba, N., Chen, X., 2005. Representative strain of indentation analysis. J. Mater. Res. 20 (8), 2225–2234.

Oliver, W.C., Pharr, G.M., 1992. An improved technique for determining hardness and elastic-modulus using load and displacement sensing indentation experiments. J. Mater. Res. 7 (6), 1564–1583.

Oliver, W.C., Pharr, G.M., 2004. Measurement of hardness and elastic modulus by instrumented indentation: advances in understanding and refinements to methodology. J. Mater. Res. 19 (1), 3–20.

Picoli, S., Mendes, R.S., Malacarne, L.C., 2003. q-exponential, Weibull, and q-Weibull distributions: an empirical analysis. Physica A-Statist. Mech. Appl. 324 (3–4), 678–688.

Smith, C.S., 1960. A History of Metallography. MIT Press, Cambridge, MA, USA, pp. 3–5.

Suresh, S., 2001. Graded materials for resistance to contact deformation and damage. Science 292 (5526), 2447–2451.

Suresh, S., 2006. Crystal deformation: colloid model for atoms. Nat. Mater. 5 (4), 253–254.

Suresh, S., Mortensen, A., 1998. Fundamentals of Functionally Graded Materials. Institute of Materials, London.

Suresh, S., Olsson, M., Giannakopoulos, A.E., Padture, N.P., Jitcharoen, J., 1999. Engineering the resistance to sliding-contact damage through controlled gradients in elastic properties at contact surfaces. Acta Mater. 47 (14), 3915–3926.

Taylor, E.S., 1974. Dimensional Analysis for Engineers. Clarendon Press, Oxford, UK.

Wang, L., Rokhlin, S.I., 2005. Universal scaling functions for continuous stiffness nanoindentation with sharp indenters. Int. J. Solids Struct. 42 (13), 3807–3832.

Williams, G., 1970. Non-sysmmetrical dielectric relaxation behaviour arising from a simple empirical decay function. Trans. Faraday Soc. 66, 80.